TWO-AXIS OPTICAL MEMS SCANNER

Shorya Awtar*, Klint A. Rose**, Hoe-Phong Tham***
*Precision Engineering Research Group, Massachusetts Institute of Technology, MA
**Mechanical Engineering, Stanford University, CA, ***Precision Engineer
shorya@mit.edu, klint@stanford.edu, thamhp@alum.mit.edu

Abstract

This paper presents the design of a two-axis optical MEMS mirror for use in raster scanning applications. The design is based on a novel resonant structure that provides two orthogonal and decoupled rotations of a single mirror. Translational errors of the mirror are eliminated by using the principle of virtual pivot in cantilever beams. The first few resonance modes and frequencies of the proposed structure are determined using a lumped-mass analysis, and validated by means of computational FEA. Appropriately placed PZT electrodes are used to excite the two modes of the structure that correspond to the rotations required for scanning. A simple fabrication process is suggested for manufacturing the device.

Keywords: Two-axis Scanner, Decoupled Rotations, Virtual Pivot

Introduction and Background

Two-axis beam steering and raster scanning MEMS mirrors are required in a broad range of applications such as biomedical imaging, scanned-beam displays and imagers, and bar code readers. While successive single axis mirrors have been frequently used to steer a beam along multiple axes [1], a more compact alternative is to use a single two-axes mirror [2-5]. Although this option simplifies the assembly, integration and packing, it often this leads to a relatively complex device design with limited performance. The bending and torsion of a single cantilevered blade has been employed to produce two orthogonal rotations of a mirror fixed at the end of the blade, thus generating the two scanning modes [2]. However, along with rotation, bending also produces blade tip translation, which can alter the alignment of the light beam being reflected and affect the optics performance. Furthermore, the same structural element is responsible for both the excitation modes, bending and torsion, thus coupling the two. Other designs employ double gimbals [3-4], which provide perfect decoupling between the two scanning axes, but also pose actuation challenges when large rotations are desired. The excitation for the second axis has to be wired through the live hinge of the first axis, which leads to fabrication and reliability concerns. Ground mounted actuation schemes such as electrostatic pads require very high voltages for the desired mirror size and range of rotations. Dual-axis MEMS mirrors that employ 3-D self-assembled structures pose obvious challenges in fabrication and packaging [5].

In the following sections, we present a new two-axis MEMS scanner design that addresses some of the key performance and fabrication issues. A simple design provides high performance while keeping the fabrication complexity low. Specifications for the scanner include a device size of 5mm x 5mm, and a mirror size of 1mm x 1mm. The two scan axes are decoupled, the scan frequencies are widely spaced (550Hz and 15.5kHz), and parasitic translational errors of the mirror are minimized. The design allows large ranges of rotations (+/-10°) while consuming less than 20mW power.

Proposed Design

The proposed structure, illustrated in Fig.1, comprises of an intermediate stage supported by two cantilever blades, an assembly that is compliant in bending but stiff in torsion. The mirror is attached to the intermediate stage by means of a bar that is stiff in bending but relatively compliant in torsion. Thus, one scan mode is produced by the bending of the cantilevers during which the intermediate stage and the mirror behave like a single rigid body along the Z axis. The second scan mode arises due to the twisting of the torsion bar. If the torsional stiffness of the cantilever blades assembly is large compared to the torsion bar and the inertia of the intermediate stage is much greater than that of the mirror, the twisting can be limited to primarily the torsion bar. The dependence of these two modes on distinct structural elements, namely the cantilevers and the torsion bar, provides the necessary decoupling between the two rotational axes.

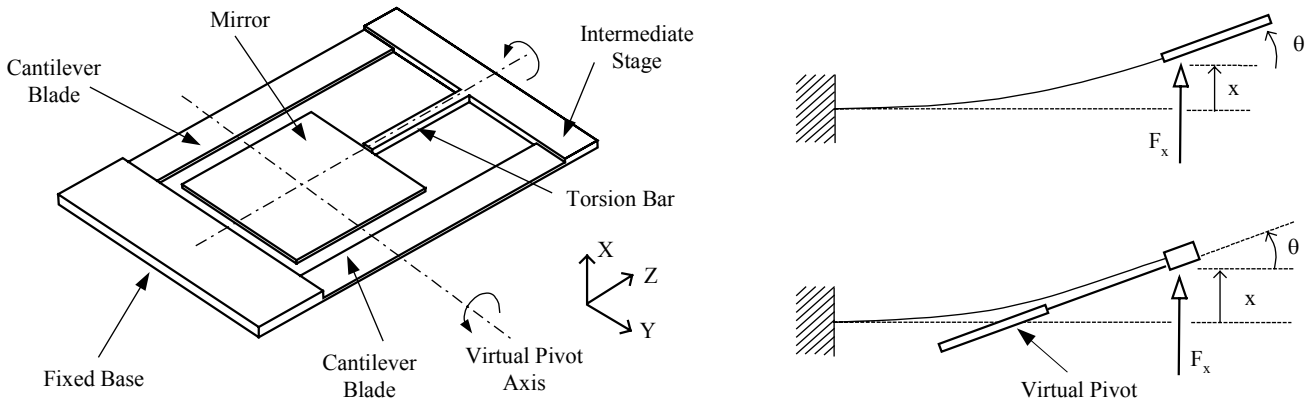

Fig.1 a) Device Concept for a 2-Axis Scanner b) Principle of Virtual Pivot

The mirror is located with respect to the intermediate stage such that its center axis coincides with the virtual center of rotation of the intermediate stage attached at the cantilever end. This arrangement eliminates any translation of the mirror center [6], as illustrated in Fig. 2. The virtual center of rotation of the intermediate stage may be determined analytically and remains fixed as long as the load-displacement behavior remains linear, damping is small, and the end loads – external or inertial, vary proportionally. In a dynamic case, for example if the cantilever is vibrating in its first natural mode, while the inertia properties of the intermediate stage and the frequency of vibration will determine the virtual pivot, its location remains fixed for small displacements.

The proposed structure may be designed so that the desired bending and torsion correspond to two distinct resonance modes, which may be exclusively excited by actuating the structure at the appropriate frequencies. Furthermore, the bending natural frequency can be considerably lowered by selecting a heavy intermediate stage. This is an important advantage because it is desirable to have the two scan frequencies separated by at least a decade to ensure optimal scanning. The torsion frequency will still be high because of the low moment of inertia of the mirror as compared to the intermediate stage. Because of close-to-resonance operation, large ranges of motion can be obtained even for small actuation signals. After evaluating several actuation schemes, PZT electrodes deposited at the base of the two cantilevers are chosen because of their rapid time response, and fabrication ease and reliability in MEMS.

System Dynamics Analysis

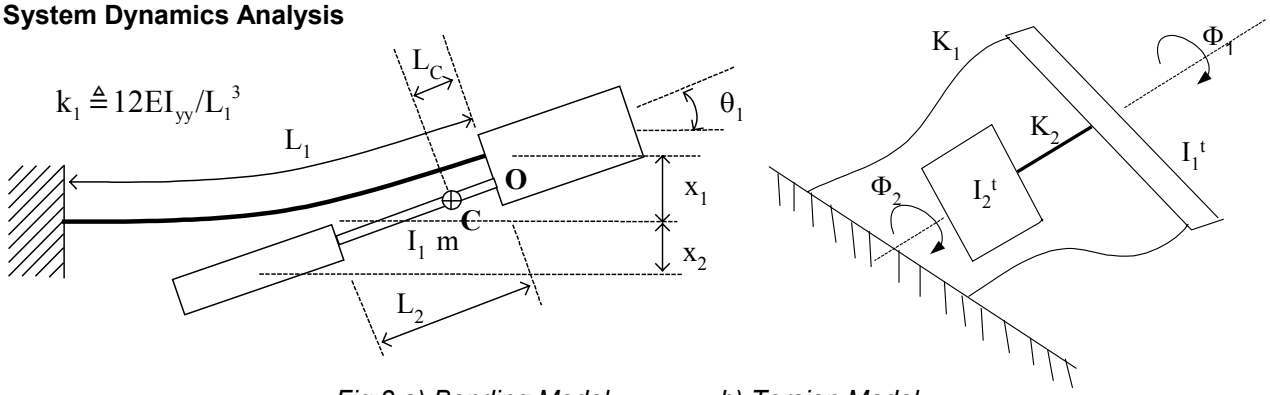

Fig.3 a) Bending Model b) Torsion Model

The objective of this exercise is to analytically predict the above-described resonance modes and frequencies so that the structure may be designed to meet the desired scanning requirements. To achieve simple closed-form results, bending and torsion of the structure are dealt with independently. In the bending and torsion models, illustrated in Fig.3, the mass of the spring elements, namely the cantilevers and the torsion bar, are neglected in comparison to the intermediate stage and mirror. For the bending model, the intermediate stage, torsion bar and mirror are assumed to be a single rigid body, with its center of mass located at C. Viscous damping is separately estimated using standard results for motion of bars and plates through air. b_1, b_2, b_3, and b_4 are the damping coefficients associated with the X translation of the intermediate stage, Y rotation of the assumed rigid body, Z rotation of the intermediate

stage, and Z rotation of the mirror, respectively. The excitations produced by the PZT electrodes at the cantilever base appear as blade tip displacement, bend angle, and twist angle, given by $x_o = L_1 c_1 V_1^{in}$, $\theta_o = c_1 V_1^{in}$ and $\phi_o = c_2 V_2^{in}$, respectively. Using the nomenclature of Fig. 3 and applying Newton's Law yields the following system dynamics.

$$\left[mI_1^{c} s^4 + (mb_2 + I_1^{c} b_1)s^3 + \left\{ mk_1 L_1 \left(\frac{L_1}{3} - L_c \right) + k_1 I_1^{o} + b_1 b_2 \right\} s^2 + \left\{ b_1 k_1 L_1 \left(\frac{L_1}{3} - L_c \right) + b_1 k_1 L_c^{2} + b_2 k_1 \right\} s + \frac{k_1^{2} L_1^{2}}{12} \right] \theta_1$$
$$= \left[m\left(L_c - \frac{L_1}{3} \right) s^2 + b_1 \left(L_c - \frac{L_1}{3} \right) s + \frac{k_1 L_1}{6} \right] \frac{k_1 L_1 c_1}{2} V_1^{in} \quad (1)$$

$$\left[\left(I_1^{o} - m\frac{L_1 L_c}{3} \right) s^2 + \left(b_2 + b_1 L_c^{2} - \frac{b_1 L_1 L_c}{3} \right) s + \frac{k_1 L_1^{2}}{6} \right] \theta_1 = \left[m\left(L_c - \frac{L_1}{3} \right) s^2 + b_1 \left(L_c - \frac{L_1}{3} \right) s + \frac{k_1 L_1}{6} \right] x_1 \quad (2)$$

$$\left[I_1^{t} I_2^{t} s^4 + \left(I_1^{t} b_4 + I_2^{t} b_3 \right) s^3 + \left(I_1^{t} K_2 + I_2^{t} (K_1 + K_2) + b_3 b_4 \right) s^2 + \left(K_2 (b_3 + b_4) + K_1 b_4 \right) s + K_1 K_2 \right] \phi_2 = K_2 \; c_2 \; V_2^{in} \quad (3)$$

The coefficient of θ_1 in the expression (1) is the characteristic polynomial of the bending system model. An order four characteristic polynomial reflects that this model captures two bending modes of the real structure. The center of rotation for a given excitation frequency may be determined from expression (2). For the designed structure geometry, the virtual pivots are found to be located at $0.35L_1$ and $1.06L_1$ from the base for the two bending modes. The coefficient of ϕ_2 in expression (3) provides the characteristic polynomial for the torsion model, and predicts two torsion modes of the real structure. Fig. 4 provides a Bode plot of the above transfer functions, and also a table that compares the predicted modes with FEM results. The derived model accurately predicts four out of the first seven modes of the structure, including the two that are of interest: simple bending of the cantilevers and pure torsion of the torsion bar.

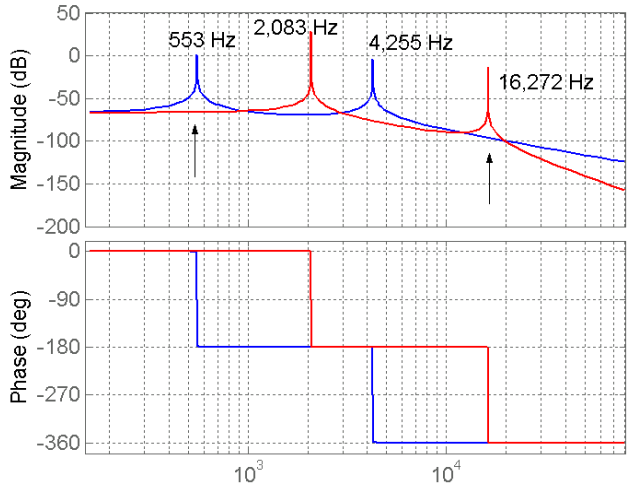

Mode	Description	FEM (Hz)	Analysis (Hz)
1	***Simple Bending of the Cantilevers***	***562***	***553***
2	Simple Torsion of the Cantilevers	2190	2083
3	Secondary Bending of the Cantilevers	3025	4225
4	In-plane Bending of the Torsion Bar	5623	
5	In-plane Bending of Cantilevers and Torsion Bar	11674	
6	Out-of-plane Bending of the Torsion Bar	12633	
7	***Pure Torsion of the Torsion Bar***	***15545***	***16272***

Fig.4 a) Analytically Predicted Bending [Blue] and Torsion [Red] Modes b) Comparison with FEM

Fabrication

The proposed fabrication plan for this device begins with an SOI wafer with a handle wafer thickness of 350μm separated by 0.5μm of silicon dioxide from the 40μm top layer of silicon. The final thickness of the scanning mirror and cantilever blades is 20 μm, and that of the torsion bar is 40 μm, which determines the thickness of the secondary silicon on the SOI wafer. The back-side of the wafer is masked and etched up to the oxide layer, which acts as an etch stop, to create the intermediate stage (Fig.5a). The next step in the process is a large area 20μm DRIE etch on the front-side leaving behind 20μm of silicon protruding from the surface for the thicker torsion bar (Fig.5b). This raised feature may cause image distortion during subsequent photolithography because the distance between the mask and photoresist would be a minimum of 20μm. The net result is an uncertainty of approximately 5μm in the torsion bar width of 75μm, which is acceptable. Next, a 250 nm silicon dioxide layer is deposited to insulate electrodes for the PZT from the silicon substrate. The oxide layer is deposited using CVD then etched in an RIE.

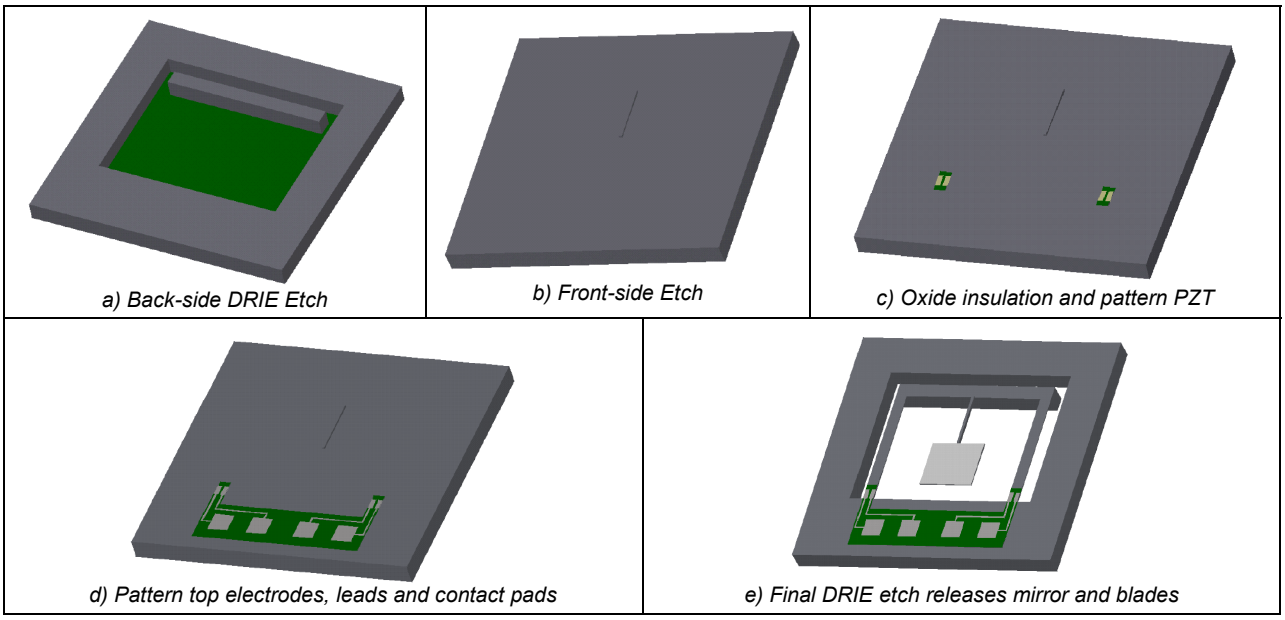

Fig.5 Key Fabrication Steps

With the insulation in place, a layer of photoresist for a lift-off process is spun on and patterned, leaving open areas on the oxide for the electrodes. A 100 Å adhesion layer of titanium is evaporated onto the oxide followed by 1000 Å of platinum. After stripping the resist, four electrodes remain which will act as the ground for voltages across the PZT. The PZT piezoelectric material is then spun on the substrate in a sol-gel form. Only thin layers of PZT, 150nm at a time, can be formed because of the condensation and annealing requirements of the material [7]. Once deposited, the PZT is masked with photoresist and patterned using a wet-etch technique [8] (Fig.5c). The leftover back-side oxide helps reduce potential undercutting during this PZT etch. Before patterning the top electrodes for the PZT, another insulating layer of oxide is necessary to avoid shorting between the top and bottom electrodes. This is performed in the same manner as earlier. The mask for the top electrodes also includes traces to a 350mm square contact pads for wire bonding to the external electronics (Fig.5d). To provide a reflective surface on the scanner mirror, evaporated aluminum is patterned onto the area using a lift-off process with a chrome adhesion layer. The final step is a DRIE etch to free up the mirror and the cantilevers (Fig.5e). The PZT actuators must be poled before use in order to maximize the strain for a given applied voltage.

Conclusion and Acknowledgement

Macro-scale and MEMS prototypes of the proposed device are currently being considered for fabrication and experimental testing. Future analytical work includes estimation of virtual pivot location errors that may arise due to other modes that get excited by the PZT actuators. Features that allow real-time frequency tuning are being investigated for design augmentation. Further information on the design, modeling, analysis, fabrication and packaging of this device can be found in a detailed report available at web.mit.edu/shorya/www. This research was conducted as part of a course project for 6.777 MEMS Design at MIT in Spring 2002, and the authors would like to thank Prof. Steve Senturia for his guidance.

References

1. D.W. Wine et al., US Patent 6,245,590 (1999)
2. H. Goto, US Patent 5828051 (1992)
3. Y. Ohtuka, H. Nishikawa, T. Koumura, T. Hattori, *IEEE Proc. MEMS'95* (1995)
4. G.-D.J. Su, H. Toshiyoshi, M.C. Wu, *IEEE Photonics Technology Letters*, **13** (2001) 606 –608
5. M.H. Kiang, O. Solgaard, K.Y. Lau, R.S. Muller, *Sensors and Actuators*, **A70** (1998) 195-199
6. A. Gonsalves, W.T. Plummer, cited in *Precision Machine Design* by A.H. Slocum (1992) 527
7. D.L. Polla, L.F. Francis, *Annual Review of Materials Science* **28** (1998) 563-597
8. L. P. Wang et al., *Mat. Res. Soc. Symp. Proc.* **657** (2001) EE5.39.1-EE5.39.6